

# Modelling of pedestrian level wind environment on a high-quality mesh: A case study for the HKPolyU campus

Yaxing Du<sup>a</sup>, Cheuk Ming Mak<sup>a\*</sup>, Zhengtao Ai<sup>b</sup>

<sup>a</sup>*Department of Building Services Engineering, The Hong Kong Polytechnic University, Hung Hom, Kowloon, Hong Kong*

<sup>b</sup>*International Centre for Indoor Environment and Energy, Department of Civil Engineering, Technical University of Denmark, Denmark*

\*Corresponding author email: [cheuk-ming.mak@polyu.edu.hk](mailto:cheuk-ming.mak@polyu.edu.hk)

## Abstract

Quality and efficiency of computational fluid dynamics (CFD) simulation of pedestrian level wind environment in a complex urban area are often compromised by many influencing factors, particularly mesh quality. This paper first proposes a systematic and efficient mesh generation method and then performs detailed sensitivity analysis of some important computational parameters. The geometrically complex Hong Kong Polytechnic University (HKPolyU) campus is taken as a case study. Based on the high-quality mesh system, the influences of three important computational parameters, namely, turbulence model, near-wall mesh density and computational domain size, on the CFD predicted results of pedestrian level wind environment are quantitatively evaluated. Validation of CFD models is conducted against wind tunnel experimental data, where a good agreement is achieved. It is found that the proposed mesh generation method can effectively provide a high-quality and high-resolution structural grid for CFD simulation of wind environment in a complex urban area.

*Keywords: Computational fluid dynamics (CFD) simulation; Pedestrian level wind environment; Mesh generation method; Complex urban environment; Sensitivity analysis.*

## **Software availability**

Software name: ANSYS Computational Fluid Dynamics (CFD) 13.0 (Pennsylvania)

Developer: ANSYS, Inc.

Contact address: South-pointe, 2600 ANSYS Drive, Canonsburg, PA 15317, USA

Fax: 724.514.9494

Program language: C/C++

Hardware requirement: Standard PC

Software Availability: The software could be purchased for academic purposes upon request.

Website: [www.ansys.com](http://www.ansys.com)

## **1. Introduction**

The pedestrian level wind environment has become a pressing issue since achieving an acceptable wind environment is unsuccessful in many urban cities, which results in many environmental problems, including thermal comfort, city ventilation and pollutant dispersion. Accurate modelling of wind flow in the urban environment is therefore crucial to wind comfort assessment, wind safety assessment, as well as thermal comfort evaluation, all of which can affect the sustainable development of a built environment (Ai and Mak, 2015; Blocken et al., 2012; Hang and Li, 2010; Juan et al., 2017; Mochida and Lun, 2008; Ng, 2009; Richards et al., 2002; Shi et al., 2015; Stathopoulos, 2006; Yuan et al., 2016). In the past decades, the pedestrian level wind environment in the urban environment has been extensively investigated by field measurement (Niu et al., 2015), wind tunnel test (Cermak, 2003; Du et al., 2017a; Tsang et al., 2012; Tse et al., 2017), and computational fluid dynamics (CFD) modelling (Blocken et al., 2016; Du et al., 2017b; Hong and Lin, 2015; Liu et al., 2016; Tominaga and Stathopoulos, 2011; Yoshie et al., 2007). Compared to the first two methods, CFD simulation has lots of advantages in studying pedestrian level wind environment, such as providing whole-flow field data, easily performing parametric study and less expensive. However, CFD simulation of urban environment has been hindered by several problems, including the difficulties of generating high-quality mesh for geometrically complex real urban community and the proper choice of important computational parameters. Therefore, works that can improve the reliability and accuracy of CFD predicted results on pedestrian level wind environment still remains of great significance.

It is well-known that the construction of high-resolution and high-quality mesh system for the complex urban environment is the prerequisite for successful simulation. Standard automatic or semi-automatic generation of unstructured grid in a complex urban environment lacks adequate control of local mesh resolution and quality, which often results in poor-quality mesh system and hinders the

accurate simulation of wind environment in urban areas. Besides, generation of unstructured grid in a large computational terrain will lead to a striking number of cells especially when the grid is required to have high density at specific location, e.g. at least 4 or 5 grid is required at pedestrian level for accurate prediction of pedestrian level wind environment (Franke et al., 2007; Tominaga et al., 2008b). The body-fitted grid generation technique presented by van Hooff and Blocken (2010) allows full control over the mesh quality and resolution when modelling a complex stadium; but it is limited to the use of unstructured prismatic cells in the computational domain. On the contrary, a high-quality structural grid can effectively reduce the cell number, save numerical cost, avoid numerical diffusion and become more stable when modelling the complex urban environment than unstructured grids (Franke et al., 2007). Therefore, a mesh generation method that can effectively produce high-resolution and high-quality structural grid with full control over the whole computational domain is in urgent need.

The time-averaging Reynolds-Averaged Navier Stokes (RANS) turbulence models are commonly used to simulate pedestrian level wind environment in urban environment among the existing turbulence models for its acceptable performance and economic computational cost (Ai and Mak, 2013, 2017; Ai et al., 2013; Baker, 2007; Bechmann et al., 2011; Blocken, 2015; Cui et al., 2016; Du et al., 2017b; Shi et al., 2015; Yoshie et al., 2007). The Realizable  $k - \varepsilon$  turbulence model was used to predict the pedestrian level wind environment at the campus of Eindhoven University of Technology and the predicted results agreed generally well with the long-term and short-term on-site measurements (Blocken et al., 2012; Janssen et al., 2013). Du et al. (Du et al., 2017b) utilized the renormalization group (RNG)  $k - \varepsilon$  model to evaluate the effects of “lift-up design” between the ground and the main building structures on the pedestrian level wind comfort in different building configurations, which aims to provide solid scientific evidence for improving weak wind conditions in Hong Kong. Even though the above studies have obtained overall good predicted results of pedestrian level wind environment by utilizing the RANS turbulence model in CFD simulation, these investigations did not conduct sensitivity tests of the computational parameters which may have major influence on the predicted results.

Owing to the widely application of CFD simulation in urban aerodynamics, a set of best practice guidelines (BPGs) are established to ensure the reliability and accuracy of the CFD predicted results (Franke et al., 2007; Jakeman et al., 2006; Laniak et al., 2013; Tamura et al., 2008; Tominaga et al., 2008b). In addition to this, a lot of studies have been conducted to improve the accuracy in CFD simulation, including achieving a homogeneous boundary layer (ABL) (Ai and Mak, 2013; Blocken et al., 2007; Gorré et al., 2009; Yang et al., 2009). While BPGs have detailed guidance on the choices

of important computational parameters, several choices are available for some important computational parameters when modelling a complex urban environment. It has been indicated that the performance of different steady RANS turbulence models are different when modelling wind flows around isolated buildings (Lateb et al., 2013; Tominaga et al., 2008a; Tominaga and Stathopoulos, 2009). Besides, the study of Ramponi and Blocken (2012) reported that the different sizes of computational domain have great influence on the cross-ventilation for a generic isolated building. Furthermore, the investigation about the effect of near-wall mesh density presented in our previous study of single-sided ventilation (Ai and Mak, 2014) showed that the near-wall mesh density can affect the predicted results of the ventilation rate. However, the sensitivity analyses of the computational parameters for CFD simulations are mainly focused on isolated buildings (Lateb et al., 2013; Lun et al., 2007; Ramponi and Blocken, 2012; Tominaga and Stathopoulos, 2009). The effects of the computational parameters on the pedestrian level wind environment based on a complex urban environment are rarely reported. In order to provide a reliable and accurate prediction of pedestrian level wind environment in a complex urban environment, a comprehensive sensitivity analysis of the important computational parameters is required.

This paper presents an investigation of improving the predicted accuracy of the pedestrian level wind environment in a complex urban environment. An effective and systematic mesh generation method is proposed in this study for generating a high-quality structural grid, which also allows full control over the grid resolution and ensures the near-wall mesh density. The proposed mesh generation method can be efficiently applied in meshing a complex urban area, as well as simple building blocks. Another prominent feature of the proposed mesh generation method is that it can ensure a sufficient near-wall mesh density without a significant increase of the total number of cells. The computational model of the HKPolyU campus is used as a case study to illustrate the mesh generation method, in which the configurations of the buildings are very complex and it has lift-up design between the ground and the main building structures (Du et al., 2017a; Niu et al., 2015). The steady RANS turbulence models are used to simulate the pedestrian level wind environment and the predicted results are validated against quality wind tunnel experimental data. Moreover, the sensitivity analysis of three important computational parameters are conducted based on the campus model, namely, turbulence model, near-wall mesh density and computational domain size.

The proposed mesh generation method is described in Section 2 with an illustration of the HKPolyU campus model. Section 3 presents the CFD simulation performance evaluation, and the guidelines of the previous studies (Bennett et al., 2013; Blocken and Gualtieri, 2012; Jakeman et al., 2006) are followed to ensure the confident numerical modelling. Firstly, the wind tunnel tests reported in Section

3.1 satisfy the requirements of ASCE and AWES (ASCE, 1999; AWES, 2001) for conducting quality wind tunnel tests. Secondly, in Section 3.2 and Section 3.3, the best practice guidelines (BPGs) (Blocken, 2015; Franke et al., 2007; Tominaga et al., 2008b) for modelling urban aerodynamics are rigorously followed throughout the simulation. Thirdly, the direct comparison method (Bennett et al., 2013) is used to assess the model performance in Section 3.4. Meanwhile, the quantitative evaluation method (Bennett et al., 2013) is used in Section 4 to analyse the sensitivity test results of the important computational parameters. Finally, concluding marks are given in Section 5.

## **2. Computational mesh**

### **2.1. Mesh generation method**

The resolution and quality of mesh system is considered crucial to accurately reproduce the wind flow in a complex urban environment, especially when modelling pedestrian level wind environment. However, generating a computational domain with high-quality and high-resolution structural grid is definitely not straightforward. Therefore, to be able to allow full control of local cells and generate a high-quality structural grid in the whole computational domain, an efficient and systematic mesh generation method is proposed here. It is a specific procedure to effectively generate high-quality structural grid in a complex urban environment and also ensures high density of near-wall mesh. The mesh generation method is schematically depicted in Fig.1. It should be mentioned that the mesh generation method presented in this study is different from the body-fitted (BF) mesh-generation technique used by van Hooff and Blocken (2010) in the following two ways: (i) the BF technique generates both prismatic cells (unstructured cells) and hexahedral cells (structural cells) in the computational domain, and the prismatic cells are used in the immediate vicinity of complex buildings. However, the mesh generation method presented by this paper can produce hexahedral cells all over the computational domain. (ii) The use of structural cells and near-wall mesh technique in this proposed mesh generation method can potentially reduce numerical cost.

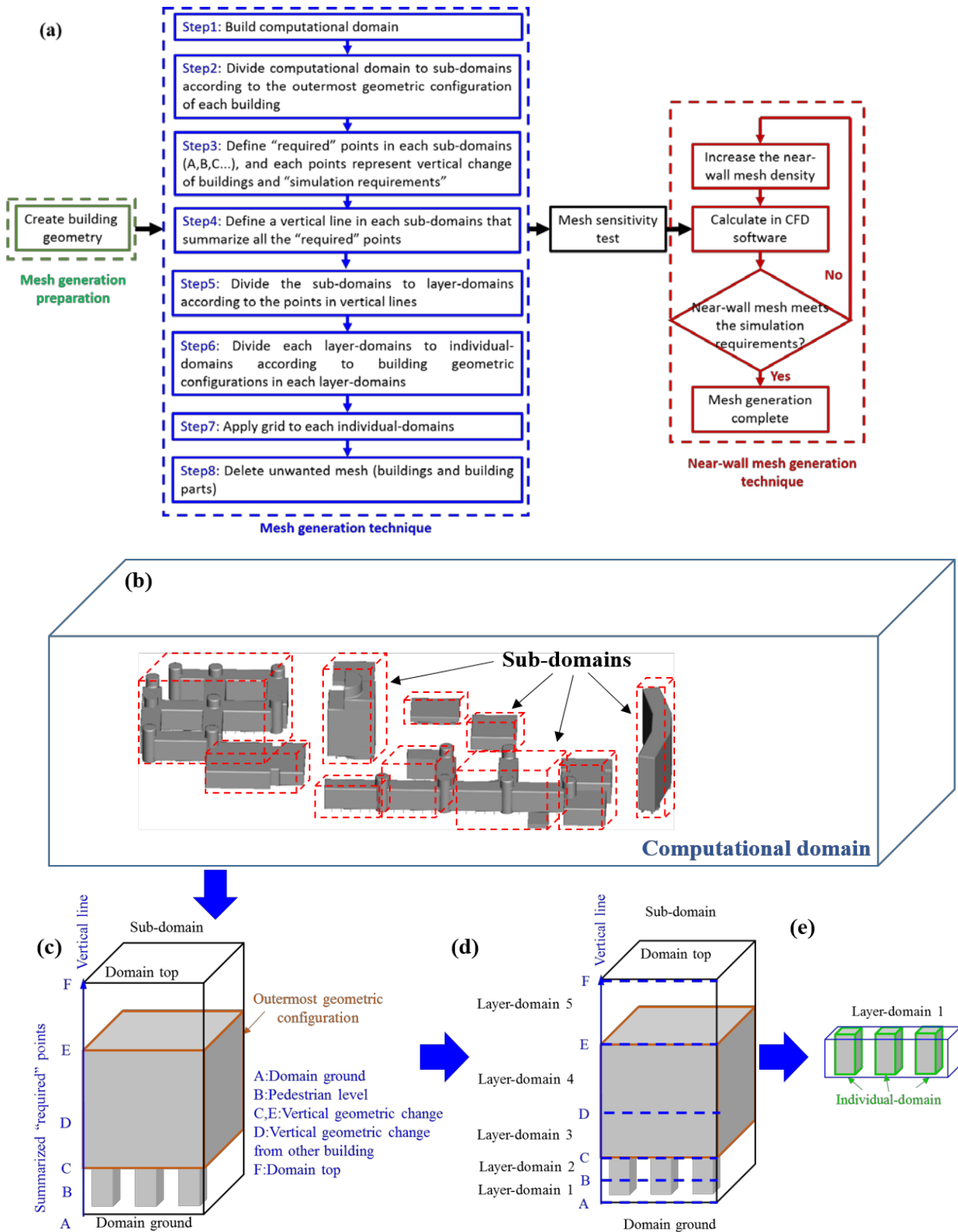


**Fig1.** (a) Flow chart of the proposed mesh generation method; (b) Schematic illustration of Step 2; (c) Schematic illustration of Step 3-Step 4; (d) Schematic illustration of Step 5; (e) Schematic illustration of Step 6.

As shown in Fig.1 (a), the mesh generation method contains three main parts: mesh generation preparation, mesh generation technique and near-wall mesh generation technique. Fig.1 (b), Fig.1 (c) and Fig.1 (d) presents the schematic illustration of the Step 2, Step 3 to Step 5 and Step 6 in Fig.1 (a), respectively. The detailed explanation for the procedure are outlined as follows:

Mesh generation preparation:

- The computational geometry should include all the buildings and obstacles that may affect the wind flow in the computational model. If necessary, the ground roughness boundary conditions should be specified appropriately.

Mesh generation techniques:

The application of this technique is schematically illustrated by using the HKPolyU campus model (Fig.1 (b)); and the detailed division process of a sub-domain is schematically illustrated by a generic “lift-up” design model (Fig.1 (c) and Fig.1 (d)) (Du et al., 2017b).

- Step 1: Building a computational domain for the target urban area. The size of the computational domain need to be chosen carefully according to BPGs (Blocken, 2015; Franke et al., 2007; Tominaga et al., 2008b), and it should be large enough to avoid artificial acceleration of the wind flow.
- Step 2: Dividing the computational domain built in Step 1 into sub-domains according to the outermost building geometric configuration, as shown in Fig1. (b). This is very important because the outermost geometric configuration ensures that all the building geometries are within one sub-domain. By doing this, the difficulties in meshing the complex urban area become meshing independent sub-domains, which is very similar as meshing isolated buildings.
- Step 3 and 4: Determining the “required” points in each sub-domain and defining a vertical line that summarizes all the “required” points. The “required” points on the vertical line (A, B...E, see Fig.1 (c)) should be chosen according to the geometric changes of each sub-domains and the “simulation requirements”. The “simulation requirements” refer to specific demand for mesh density vertically. For instance, this paper focuses on the pedestrian level wind environment and at least four to five cells should be applied at pedestrian level according to the BPGs. Thus, point B is defined in the vertical line.
- Step 5: Dividing the sub-domains into layer-domains according to all the points in the vertical line. It should be mentioned that the sub-domains should be divided according to all the

“required” points in the computational domain instead of the “required” points in one sub-domain.

- Step 6: Dividing the layer-domains to individual-domains according to the building geometric configuration (Fig.1 (d)). This step requires considerable patience and time, since it relates to the accurate reproduction of building geometry.
- Step 7 and 8: Applying grid to each individual-domains and deleting the unwanted mesh. This way, only the spaces that are outside buildings are meshed and the local grid quality can be ensured.

Near-wall mesh generation technique:

- It is noted that the independence of mesh resolution in the whole computational domain is the prerequisite for using near-wall mesh generation technique.
- The near-wall mesh is increased by only doubling the first cell in both horizontal and vertical directions and there will be no change to other non-near wall cells, which has been utilized in our previous study (Ai and Mak, 2014). The schematic view of the near-wall mesh generation technique and the conventional mesh generation technique are shown in Fig.2 (a) and Fig.2 (b), respectively. It has been proven to be effectively reducing numerical cost for achieving the same near-wall mesh density compared to conventional mesh generation technique that has the same stretching ratio from the first cell in the whole computational domain.

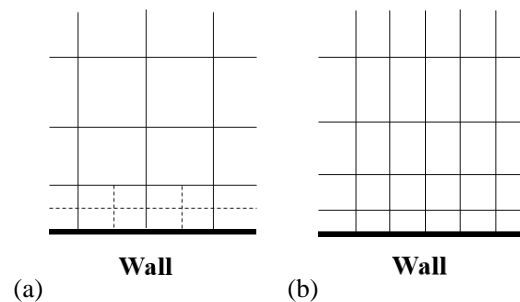


**Fig.2.** Schematic view of two techniques to change near-wall mesh density: (a) near-wall mesh generation technique; (b) conventional mesh generation technique.

The advantages of this mesh generation technique are: (i) it is a systematic and efficient procedure for generating structural cells in the whole domain. (ii) It allows full control over the mesh generation procedure and assures the resolution and quality of local cells, which provides the prerequisite for accurately modelling wind environment in complex urban area. (iii) The structural cells in the whole computational domain and the near-wall mesh generation technique will effectively reduce the numerical cost. The proposed mesh generation method was executed with the aid of pre-processor

ICEM 13.0 (ICEM, 2010). In addition, this proposed mesh generation method can be used in other pre-processors, e.g., GAMBIT, PointWise etc.

## 2.2 Case study: the HKPolyU campus

### 2.2.1 Computational model

The HKPolyU campus model is utilized to illustrate the application of the proposed mesh generation method. The campus is located in midtown of Hong Kong with an area about 500m by 280m (as shown in Fig.3), where all the buildings are closely arranged and have complicated geometric configurations which includes lift-up design between the ground and the main building structures. It consists of high-rise and low-rise buildings and the heights of main buildings are indicated in Fig.3. It is noted that the buildings in the campus are labelled in letters: A, B, C ... Y, which represent different building cores in the campus. The building that is located between two cores is known as “building wing”, such as the building between D core and E core is “DE wing”. As for the building heights, the high buildings are M building (65.7m) and Y building (58.4m) while the low buildings are VS building (8.9m) and VA building (9.3m). The average height of building cores in the campus is 36.1m. Besides, there are two large courtyards below the ground in the campus that have significant influence on the pedestrian level wind environment: one is surrounded by PQ wing, QR wing and M building; and the other is surrounded by CD wing, DE wing, EF wing and CF wing. The average depths of the caves are 7m. The buildings and caves in the campus are all explicitly included in the computational model. It should be mentioned that the computational model of the campus is constructed in 1:200 scale which is the same scale as the wind tunnel test model since the wind tunnel test results will be used for validation. The geometrical complexity of the campus is modelled in great detail in the computational model, any configurations more than 1m in prototype were reproduced. The computational model was generated directly from the construction drawings of the campus since the data with such high resolution at pedestrian level were not available from GIS or city database. The lift-up design between the ground and the main building structures is a very distinctive building features in the campus with average height of 4 meters, which provides shielding effect from solar radiation in the hot summer and also enhances wind velocity at pedestrian level (Du et al., 2017a; Liu et al., 2016; Niu et al., 2015). Thus, it is necessary to reproduce the geometry configurations in the computational model and apply high-resolution and high-quality grid in the lift-up area.

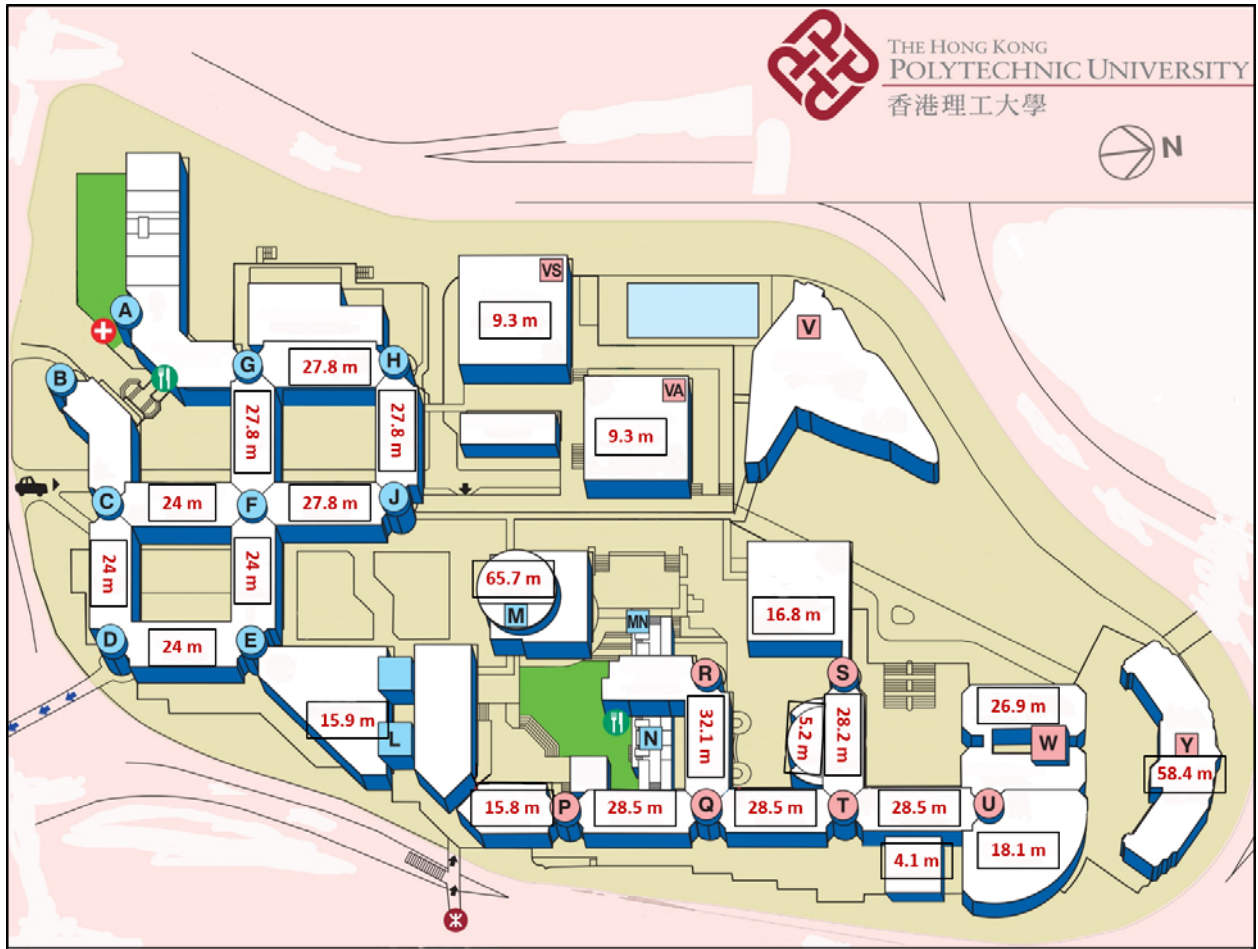


**Fig.3.** Overview of the buildings at the HKPolyU campus and the heights of main buildings.

### 2.2.2 Computational grid

Obviously, the campus is a very complex urban area and the proposed mesh generation method is therefore utilized to construct the mesh of the campus model. It should be mentioned that the vegetative elements are not included in the computational mesh. Since this study focuses on pedestrian level wind environment, special attention is paid to the building configuration at pedestrian level during the meshing process. Overviews of the mesh from eastward and its corresponding image from Google map are presented in Fig.4 (a) and Fig.4 (b), respectively. The computational mesh in Fig.4 (a) consists of 8.9 million cells. It can be seen from Fig.4 that the computational grid has high-quality and high-resolution all over the computational campus terrain, and a maximum stretching ratio of 1.18 outside the campus model (1.2 in Ramponi and Blocken, 2012). As shown in Fig.4, the top structures of building M and Y are not entirely included in the computational model. This is because these top structures are located at a relatively large distance from the pedestrian level (around 70 m in prototype), which have slight influences on pedestrian level wind environment. Besides, some differences in building models can be observed between Fig.4 (a) and Fig.4 (b), and the newly built V block is not

included in the computational model. The reason is that the simulation results in this study will be compared with wind tunnel test results for validation (see Section 3.1). Thus, the computational model is built based on the model used during the wind tunnel tests.

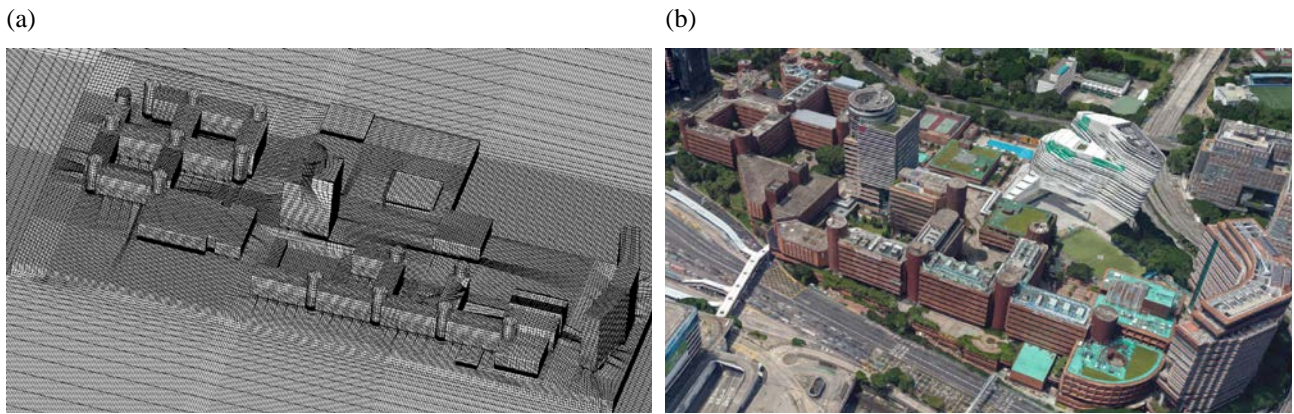


**Fig.4.** (a) Overview of high-quality computational mesh of the campus model (8.9 million cells). (b) Satellite image of HKPolyU campus from Google Map (accessed on 30 Jun. 2017).

The specific view of the computational cells for lift-up design and its corresponding photos are presented in Fig.5. As indicated in Fig.5, the quality and resolution of computational cells in lift-up area are very high, which provide the prerequisite for accurately reproducing wind flow at pedestrian level in the lift-up area. Besides, it can also be observed in Fig.5 that at least ten cells have been applied over the height of the lift-up, which suggests that there are over five cells at pedestrian level. This fulfils the requirement recommended by BPGs (Franke et al., 2007; Tominaga et al., 2008b) that the pedestrian level should be located at third or higher cell above the ground when modelling pedestrian level wind environment in an urban area.

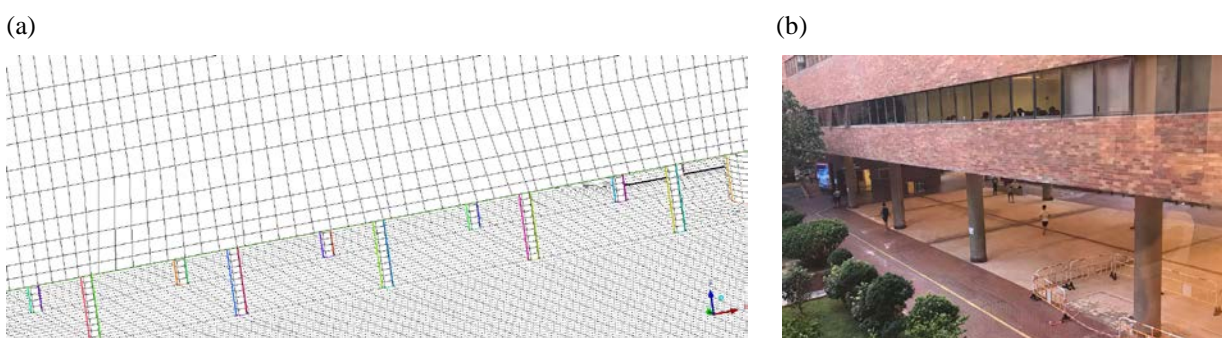


**Fig.5.** (a) High-quality computational mesh for lift-up design in the campus. (b) Photo of lift-up design in the campus.

### 3. CFD validation: basic case

#### 3.1 Wind tunnel test

For validation purpose, the wind tunnel tests of the campus model were conducted at a scale of 1:200 in the CLP power Wind/Wave Tunnel Facility (WWTF) at Hong Kong University of Science and Technology (HKUST). The blockage ratio of the test is 2.2%, which is less than 10% and the constraining effects were minimized in this test (ASCE, 1999). During the tests, the Reynolds Number ( $Re$ ) was over  $7.8 \times 10^4$ , which can be considered as sufficiently large enough to obtain  $Re$  independence (AWES, 2001). The wind tunnel test photo of the campus model and the wind profile used during the test are shown in Fig.6. It can be observed from Fig. 6(a) that the campus model was reproduced in great detail. The wind profiles in Fig.6 (b) and Fig.6 (c) are adopted from our previous study (Du et al., 2017a) and the error shown in the figures are within 5%, which suggests the reliability of the measurements.

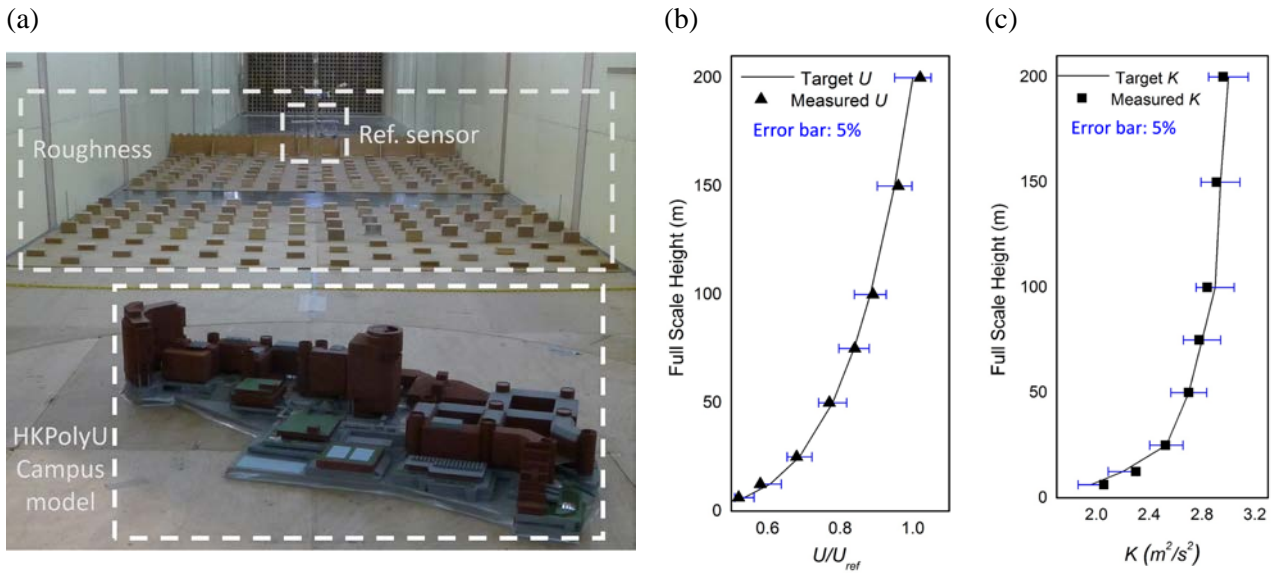


**Fig.6.** (a) Wind tunnel test photo of the campus model: approaching wind direction  $90^\circ$  (wind from east); (b) Approaching profile of mean wind velocity; (c) Approaching profile of turbulence kinetic energy.

As shown in Fig.7, 50 tests points at pedestrian level (0.01m above podium floor in scaled model and 2m in prototype) were used in this study for measurements. It can be observed that the test points were evenly distributed in the campus. The blue dots are test points located on the podium floor (labelled in letter P) and the orange dots are the test points located in the lift-up area (labelled in letter L). The blue dashed areas in Fig.7 are the lift-up areas in the campus. The Kanomax velocity sensors were used during the wind tunnel tests. The measuring frequency of the sensor was 10HZ, and the sampling time was set to be two minutes (one hour in reality). As indicated in our previous study ((Du et al., 2017a), the sensors were calibrated against a reference sensor prior to the measurement, and the largest discrepancies between the Kanomax velocity sensors and the reference sensors were within 5%.

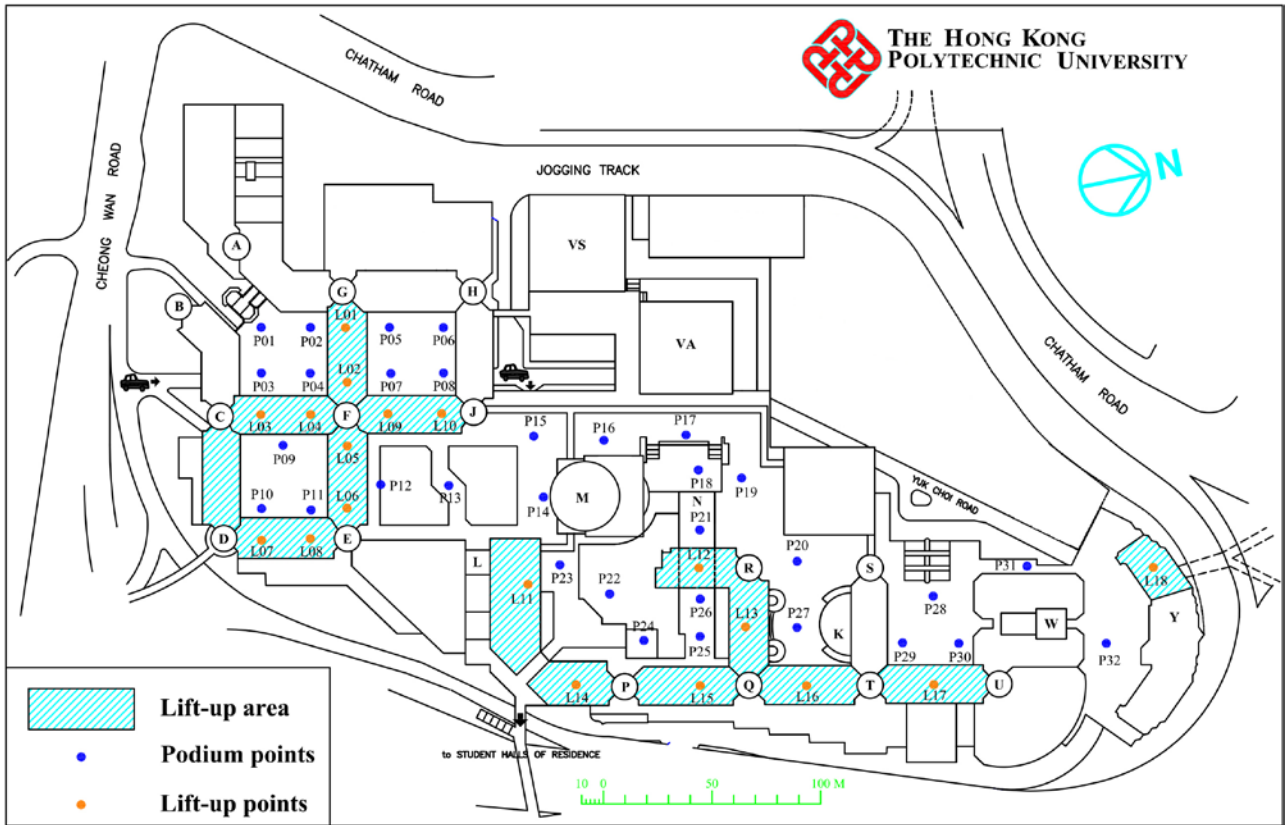


**Fig.7.** Sensor locations of the HKPolyU campus model.

### 3.2 Computational domain

The length of upstream domain should be kept as short as possible to avoid unintended stream-wise gradients, while still fulfil the recommendations of BPGs. The length of downstream should be taken long enough to assure the fully development of wind flow in the domain outlet. The dimensions of lateral side and domain height should be chosen carefully to avoid the occurrence of artificial acceleration due to the close distance between the lateral domain and building models. In this study,  $5B_H$  ( $B_H$  is the height of highest building in the campus) is chosen for the upstream length and  $22 B_H$  is chosen for the downstream length. The domain lateral and the domain height of the this case are chosen based on directional blockage ratio (DBR) (Blocken, 2015), which is the decomposition of limit value 3% in lateral horizontal and vertical direction. Since the square root of 3% is 17%, the following equations can be established:

$$Lateral_{BR} = L_{building}/L_{domain} \leq 17\% \quad (1)$$

$$Vertical_{BR} = H_{building}/H_{domain} \leq 17\% \quad (2)$$

where,  $BR$  stands for blockage ratio.  $L$  is length and  $H$  is height.

It is obvious that Eq. (1) and Eq. (2) can automatically satisfied the maximum blockage ratio of 3% recommended by BPGs (Franke et al., 2007; Tominaga et al., 2008b). Noted that in this study, only east wind direction is considered. The schematic view of the computational domain is presented in Fig.8, the domain dimensions are  $L \times W \times H = 14.41m \times 14.5m \times 2.57m$  for east wind direction.

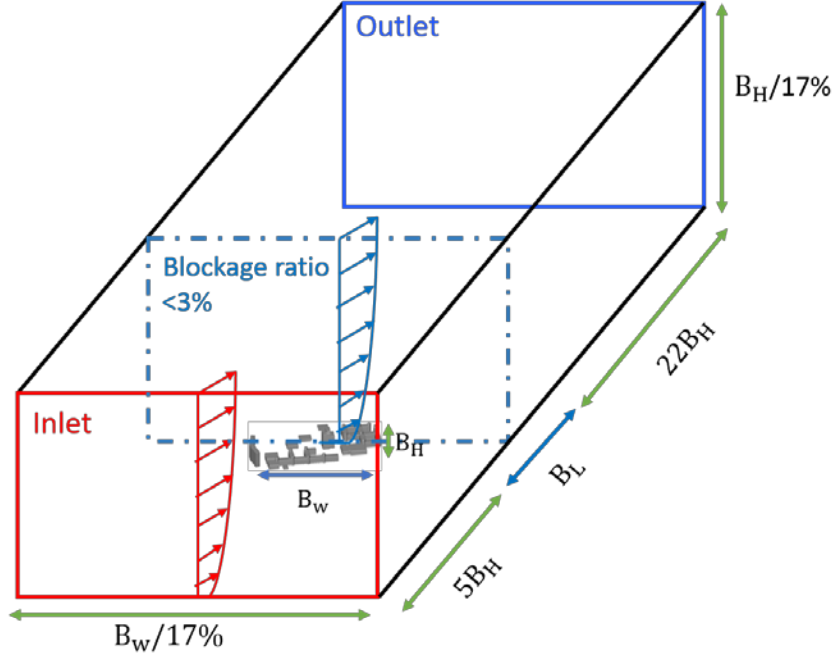


**Fig.8.** Schematic view of the computational domain for east wind direction.

### 3.3 Boundary conditions and other computational settings

The inlet boundary profiles of mean wind velocity  $U$ , turbulence kinetic energy  $k$  and turbulent dissipation rate  $\varepsilon$  are specified by Eq.(3) – Eq.(5), which are considered as capable of assuring a homogenous boundary layer when combined with proper near-wall treatment on the domain ground. The aerodynamic roughness height  $z_0$  and the friction velocity  $u^*$  are determined by fitting Eq. (3) to the measured  $U$  profile in Fig.6 (b), which results in  $z_0=0.0001$  m and  $u^*=0.2998$  m/s. The coefficients  $M_1$  and  $M_2$  are obtained by fitting Eq. (4) to the test data of  $k$  profile in Fig.6 (c), and  $M_1 = 0.97$ ,  $M_2 = 6.23$ .  $\kappa$  is the von Karman constant, which equals to 0.4187. The constant  $C_\mu$  is defined empirically as 0.09.

$$U = u^*/\kappa \times \{(z + z_0)/z_0\} \quad (3)$$

$$k = \sqrt{M_1 \cdot \ln(z + z_0) + M_2} \quad (4)$$

$$\varepsilon = \{u^* \sqrt{C_\mu}/\kappa(z + z_0)\} \cdot \sqrt{M_1 \cdot \ln(z + z_0) + M_2} \quad (5)$$

Zero normal velocity and zero normal gradients are used on the domain ceiling and domain lateral, and zero static pressure is used on the domain outlet. As for the domain ground, the two-layer model is utilized (Ai and Mak, 2013; Durbin et al., 2001). It should be mentioned that the homogeneity of these boundary conditions is examined by comparing the inlet and incident profiles in an empty computational domain before commencing CFD simulation. The results of the homogeneity examination are shown in Fig.9, and it can be seen that a good homogenous boundary layer has been achieved.

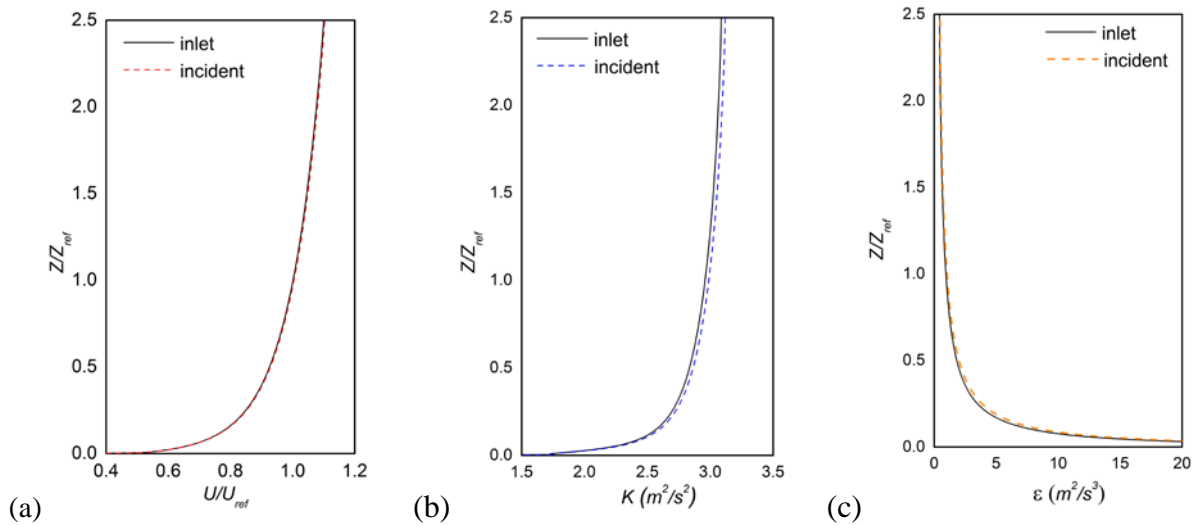


**Fig.9.** Results of homogeneity examination in an empty computational domain: (a) mean wind velocity  $U$ ; (b) turbulence kinetic energy  $k$  ; (c) turbulent dissipation rate  $\epsilon$ .

The numerical simulation is carried out by CFD code Fluent 13.0.0 (FLUENT, 2010), combining with a series of user-defined functions (UDF). The renormalized group (RNG)  $k - \epsilon$  model is utilized to predict wind flow field because of its general good performance on predicting pedestrian level wind environment (Ai and Mak, 2013; Blocken et al., 2016; Du et al., 2017b; Tominaga and Stathopoulos, 2009). The discretization of the governing equations is conducted on a staggered grid system to algebraic equations which is based on the finite volume method (FVM). The equations of momentum and pressure are coupled by the SIMPLEC algorithm with second-order upwind scheme. The convergence of the simulation is achieved when all the scaled residuals are less than  $10^{-5}$  and the monitored wind velocities at pedestrian level are stable for over 50 iterations (Ai and Mak, 2014). It should be mentioned that 16 measuring points in Fig.7 are monitored during the simulations: 8 points in the lift-up area and 8 points in the podium area. The simulations are considered converged when all the monitored points are stable for over 50 iterations.

Apart from the basic mesh with 8.9 million cells (as shown in Fig.10 (a)), one coarser mesh and one finer mesh are also constructed, containing about 6.3 million and 12.2 million cells, respectively. The predicted results of three mesh systems is shown in Fig.11. It can be seen that the prediction differences between basic mesh and coarse mesh are obvious while the prediction differences between basic mesh and fine mesh are subtle. Taking the computational cost and the accuracy of the simulation into consideration, the basic mesh is used for the following simulations.

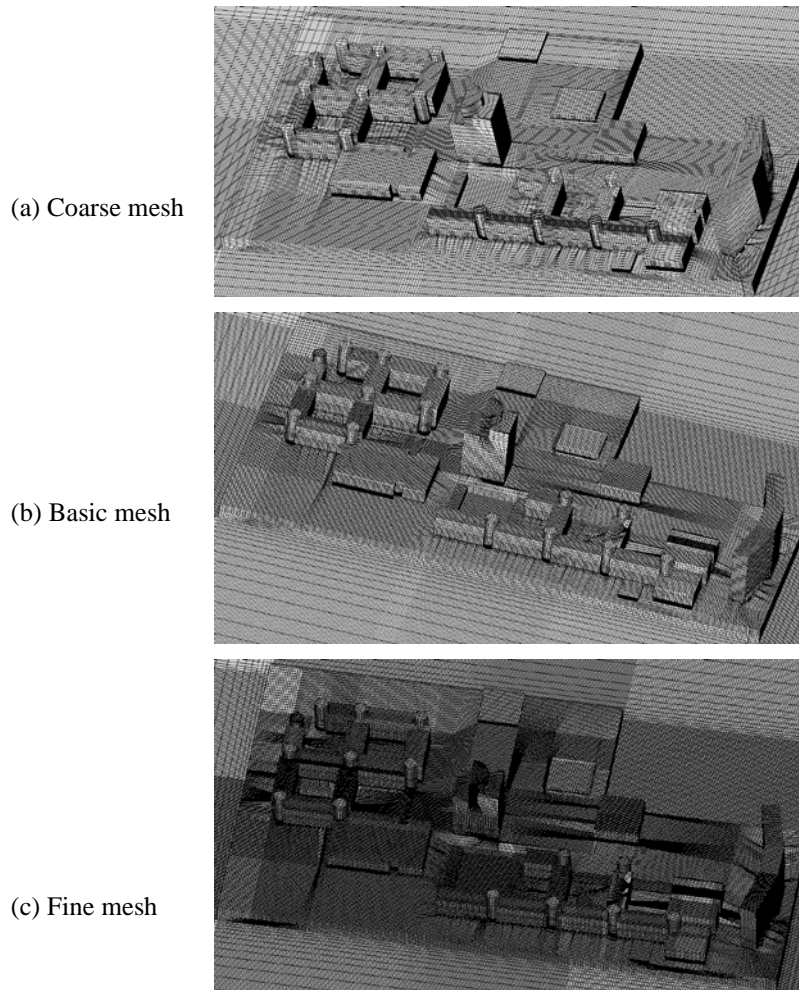


**Fig.10.** Three mesh system: (a) Coarse mesh; (b) Basic mesh; (c) Fine mesh.

(a)

(b)

**Fig.11.** Comparison results of three mesh systems: (a) Coarse and basic mesh; (b) Fine and basic mesh.

After the mesh sensitivity test of the computational model, the aforementioned near-wall mesh generation technique (as shown in Section 2.1) is utilized here to obtain the suitable near-wall mesh density for simulation requirements. It is noted that after second increase of near-wall mesh, the average values of  $y^+$  equals to 4.2 and results in 11.3 million cells, which is good enough for two layer model (Ai and Mak, 2013).

#### 3.4. Validation results

The normalized mean wind parameter, mean wind velocity ratio (*MVR*) which has been used in our previous studies (Du et al., 2017a; Du et al., 2017b), is adopted here to evaluate wind environment at pedestrian level. The definition of *MVR* is shown as follows:

$$MVR = U_p/U_r \quad (6)$$

where,  $U_p$  is the mean wind velocity at pedestrian level;  $U_r$  denotes the mean wind velocity at reference height, which is 200m in prototype and 1m in model scale.

The predicted results and the corresponding wind tunnel test data are shown in Fig.12. It can be observed that a good agreement is achieved and the deviations are almost within 20% between the predicted and measurement results. Actually, over 70% measuring points are within the deviation of 10%, which can be considered sufficiently accurate for predicting pedestrian level wind environment.

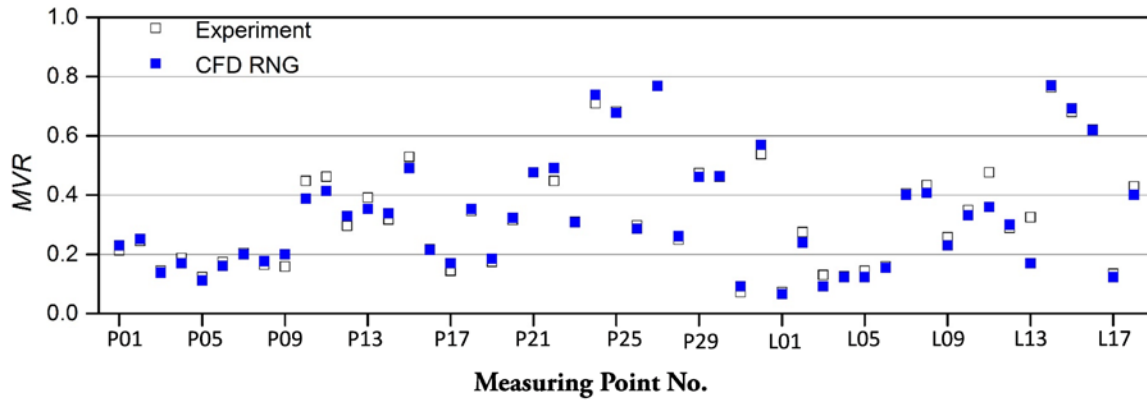


**Fig.12.** Comparison between wind tunnel test measurement results and basic case predicted results.

### 3.5 Pedestrian level wind environment

Fig.13 presents the predicted results of pedestrian level wind environment in the campus model when the approaching wind comes from east. According to the Planning Department of HKSAR, the annual average wind velocity at 200m reference height is 5m/s and the prevailing wind direction is east direction (HKSAR). Thus, the wind environment shown in Fig.13 can generally represent the annual wind environment at pedestrian level in the campus. To be able to reach the minimum wind velocity of 1.5m/s, which is the minimum threshold value of acceptable wind comfort in summer according to the wind comfort criteria proposed by the authors (Du et al., 2017a) and also meets the requirement of air ventilation assessment (AVA) scheme in Hong Kong (Ng, 2009), an *MVR* value equal or over 0.3 is required to achieve acceptable wind environment. On the contrary, areas with *MVR* values below 0.3 are designated as low wind environment as illustrated in Fig.13 (Du et al., 2017b). It can be observed that a large portion of the campus has low wind environment at pedestrian level, especially on the southward and westward side of the campus. Meanwhile, the east and middle parts of the campus have relatively higher wind velocity, which can be considered as acceptable wind environment. Besides, it can be obtained that the lift-up areas in the campus have higher wind environment at pedestrian level than the podium areas, which corresponds with our earlier findings that the lift-up design can enhance the pedestrian level wind comfort in low wind environment (Du et al., 2017a; Du et al., 2017b).

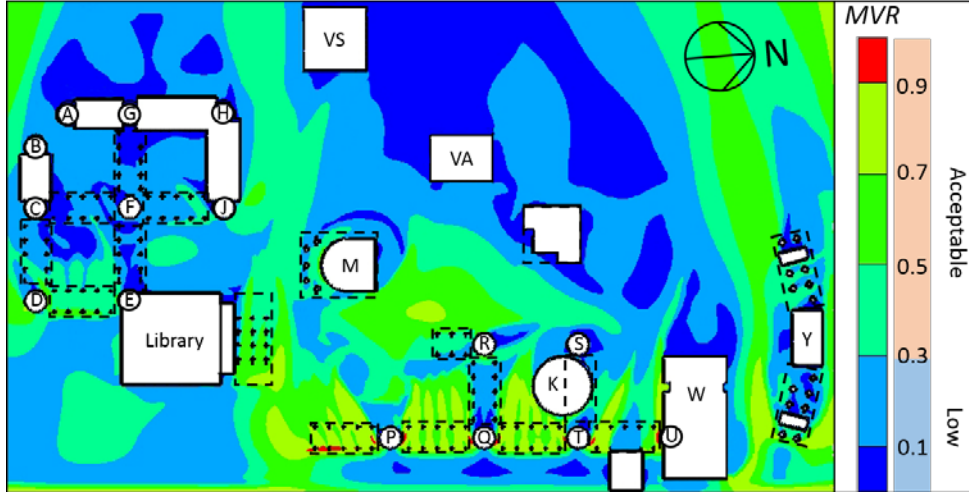


**Fig.13.** Pedestrian level wind environment of the campus model: approaching wind direction  $90^\circ$  (wind from east).

#### 4. Sensitivity analysis

As mentioned before, it is worth noting that the computational parameters of turbulence models, near-wall mesh density and computational domain size are important for accurately predicting pedestrian level wind environment, especially in a complex urban area. This section reports on detailed analysis of the above computational parameters, which can also be applied to other urban regions.

In order to quantitatively evaluate the effects of these parameters, two commonly used residual criteria: mean absolute percentage error (*MAPE*) and root mean square error (*RMSE*) (Bennett et al., 2013), are adopted here. These criteria are chosen because of the fact that *MAPE* can provide an evaluation of mean predicted errors without cancellation and *RMSE* is a measure of evaluating the overall deviation between predicted results and measured results. The definitions of *MAPE* and *RMSE* are shown as follows:

$$MAPE = (1/n) \sum_{i=1}^n |(\widehat{MVR}_i - MVR_i) / \widehat{MVR}_i| \times 100\% \quad (7)$$

$$RMSE = \sqrt{(1/n) \sum_{i=1}^n (\widehat{MVR}_i - MVR_i)^2} \quad (8)$$

here,  $n$  is the total number of evaluation points;  $\widehat{MVR}_i$  stands for measured result for the same location;  $MVR_i$  denotes predicted result of a specific location.

##### 4.1 Effects of turbulence model

The selection of a suitable turbulence model is crucial for accurately predicting the pedestrian level wind environment since the reproduction of the flow structure in a built environment is strongly

affected by the turbulence model. In this section, four types of steady RANS turbulence model in the  $k - \varepsilon$  family are used to predict the wind flow in the computational model, i.e., the standard  $k - \varepsilon$  turbulence model ((Launder, 1972); hereafter SKE), the RNG  $k - \varepsilon$  turbulence model ((Yakhot et al., 1992); hereafter RNG), the MMK  $k - \varepsilon$  turbulence model ((Tsuchiya et al., 1997); hereafter MMK) and the Realizable  $k - \varepsilon$  turbulence model ((Shih et al., 1995); hereafter RLZ). The transport equations of turbulence kinetic ( $k$ ) and dissipation rate ( $\varepsilon$ ) for the above turbulence models have similar expressions, which are shown in Eq. (9) – (11). The equations of eddy viscosity for each turbulence model also have similar forms (see Eq. (11)), but the methods for calculating turbulent viscosity are different. Besides, the turbulent Prandtl numbers and the generation or destruction terms of  $\varepsilon$  are different in each turbulence model. The major differences for each model are summarized in Table.1.

$$\frac{\partial k}{\partial t} + u_i \frac{\partial k}{\partial x_i} = \frac{\partial}{\partial x_j} \left( \frac{\nu_t}{\sigma_k} \frac{\partial k}{\partial x_j} \right) + P_k - \varepsilon \quad (9)$$

$$\frac{\partial \varepsilon}{\partial t} + u_i \frac{\partial \varepsilon}{\partial x_i} = \frac{\partial}{\partial x_j} \left( \frac{\nu_t}{\sigma_\varepsilon} \frac{\partial \varepsilon}{\partial x_j} \right) + \varepsilon/k (C_{1\varepsilon} P_k - C_{2\varepsilon} \varepsilon) \quad (10)$$

$$\nu_t = C_\mu (k^2/\varepsilon) \quad (11)$$

**Table.1.** Differences for each turbulence model

Turbulence model	Turbulence kinetic ( $k$ )	Dissipation rate ( $\varepsilon$ )	Eddy viscosity ( $\nu_t$ )
Standard $k - \varepsilon$ (SKE)	$P_k = \nu_t S^2, \sigma_k = 1$	$C_{1\varepsilon} = 1.44, C_{2\varepsilon} = 1.92, \sigma_\varepsilon = 1.3$	$C_\mu = 0.09$
RNG $k - \varepsilon$ (RNG)	$P_k = \nu_t S^2, \sigma_k = 1$	$C_{1\varepsilon} = 1.42 - \frac{\eta(1 - \eta/4.38)}{1 + 0.012\eta^3}$ $\eta = S(\frac{k}{\varepsilon}), C_{2\varepsilon} = 1.68, \sigma_\varepsilon = 0.719$	$C_\mu = 0.09$
MMK $k - \varepsilon$ (MMK)	$P_k = \nu_t S^2, \sigma_k = 1$	$C_{1\varepsilon} = 1.44, C_{2\varepsilon} = 1.92, \sigma_\varepsilon = 1.3$	$\nu_t = FC_\mu k^2/\varepsilon,$ $F = \min(\Omega/S; 1)$
Realizable $k - \varepsilon$ (RLZ)	$P_k = \nu_t S^2, \sigma_k = 1$	$\frac{\partial \varepsilon}{\partial t} + u_i \frac{\partial \varepsilon}{\partial x_i} = \frac{\partial}{\partial x_j} \left( \frac{\nu_t}{\sigma_\varepsilon} \frac{\partial \varepsilon}{\partial x_j} \right) + C_{1\varepsilon} S \varepsilon - C_{2\varepsilon} \frac{\varepsilon^2}{k + \sqrt{\nu \varepsilon}}$ $C_1 = \max[0.43, \frac{\eta}{\eta+5}], C_2 = 1.9, \sigma_\varepsilon = 1.2$	$C_\mu = \frac{1}{4.04 + A_s k U^*/\varepsilon}$ $U^* = \sqrt{S_{ij} S_{ij} + \tilde{\Omega}_{ij} \tilde{\Omega}_{ij}}$ $A_s = \sqrt{6} \cos \phi$

The predicted results of each turbulence model are presented in Fig.14, except the results of RNG, which have been shown in Fig.12. It can be observed that the predicted results obtained by all RANS turbulence models agree generally well with wind tunnel measurement results. The predicted results

given by SKE show the largest discrepancies with the measurement results among all the turbulence models, because of its incapability of reproducing the flow structure in a built environment (FLUENT, 2010; Franke et al., 2007; Tominaga and Stathopoulos, 2009). The results predicted by MMK display an overall good agreement with the wind tunnel measurements but most of the predicted results are overestimated. The predicted results produced by RNG have good agreement with wind tunnel measurements, which has been explained in Section 3.4. Even though there are some large discrepancies in Fig.14 (c), the predicted results obtained from RLZ are generally agrees very well with the wind tunnel measurements.

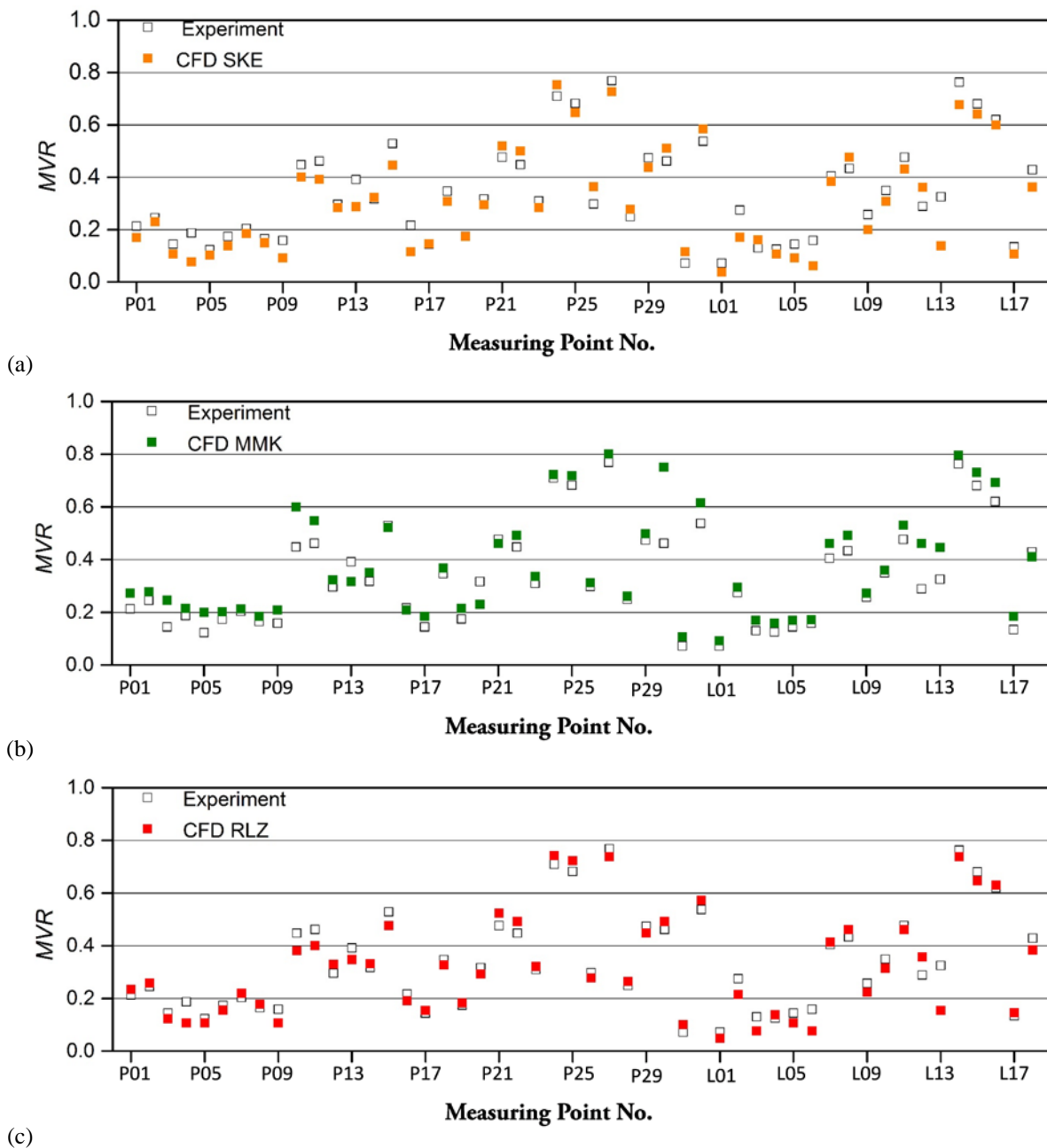


**Fig.14.** Predicted results for each turbulence models: (a) SKE; (b) MMK; (c) RLZ.

To be able to quantitatively assess the predicted performance of each turbulence model, the predicted errors for each turbulence model are given in Table 2. It can be seen that the *MAPE* and *RMSE* results obtained by RNG are smallest among the turbulence models, which suggested that the results predicted by RNG are closest to the wind tunnel measurements. The second best result is given by RLZ, and it is followed by MMK and SKE. Thus, the RNG yields the best simulation performance on the campus model among the four turbulence models.

**Table 2.** Predicted errors for each turbulence model

Turbulence model	SKE	RNG	MMK	RLZ
<i>MAPE</i> (%)	18.6	9.4	11.8	11.4
<i>RMSE</i> (m/s)	0.060	0.034	0.054	0.043

#### 4.2 Effects of near-wall mesh density

The near-wall mesh generation technique is achieved by doubling the first near-wall cell, which aims to potentially save computational cost while obtaining the desired  $y^+$  value at pedestrian level. The prerequisite for using this technique is the independence of the mesh resolution in the whole computational domain (as presented in Section 2.1 and Section 3.3). This section tests this method based on the results of HKPolyU campus model in Section 3. In addition to the case in Section 3 which has an average  $y^+$  value of 4.2 at pedestrian level, one lower value ( $y^+ = 1.9$ ) and two larger values ( $y^+ = 8.3, 18.1$ ) are investigated in this section. The increases in near-wall mesh density with the average  $y^+$  values from 18.1 to 1.9 are schematically shown in Fig.15. It can be observed that the cells increase 0.9 million, 2.5 million and 6.1 million when the average  $y^+$  values decrease from 18.1 to 8.3, 8.3 to 4.2 and 4.2 to 1.9, respectively. These results demonstrate that the near-wall mesh technique can achieve an ideal  $y^+$  value while not causing a substantial grid number increase.

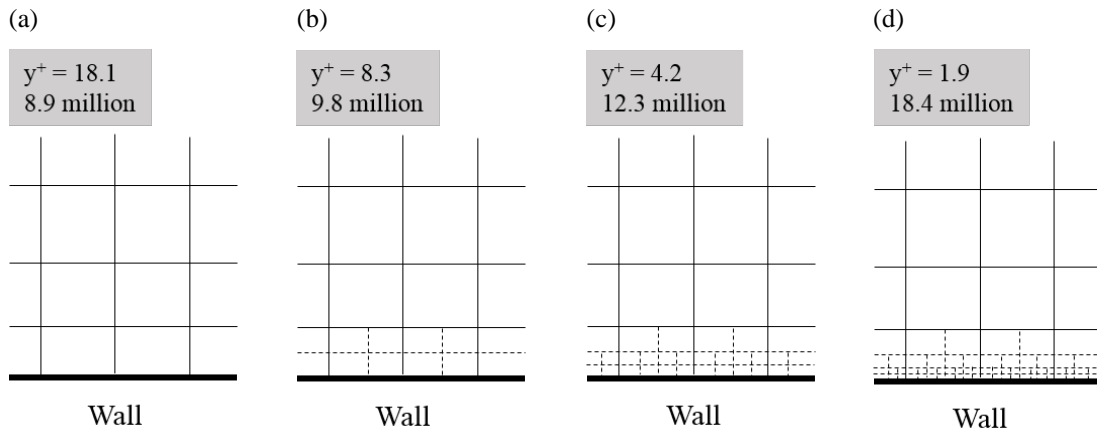


**Fig.15.** Schematic view of the near-wall density increase and mesh number: (a)  $y^+=18.1$ ; (b)  $y^+=8.3$ ; (c)  $y^+=4.2$ ; (d)  $y^+=1.9$ .

Fig.16 shows the predicted results obtained from different near-wall densities. There are no obvious discrepancies between different near-wall densities (different  $y^+$  values) because the first cells are all located within the inner layers ( $y^+ < 30$ ). The predicted results obtained from the cases of  $y^+=4.2$  and 1.9 are almost the same, and these results are more accurate than that of the cases of  $y^+=18.1$  and 8.3. This is because the two-layer model is used when the first cells are located in the viscous sublayer ( $y^+ < 5$ ) (Ai and Mak, 2013; FLUENT, 2010). Even though the increase of near-wall density does not yield significant improvement in the predicted accuracy, the decrease of the  $y^+$  values shows the feasibility of using transit turbulence models, e.g., Detached Eddy Simulation (DES) model and Large Eddy Simulation (LES) model.

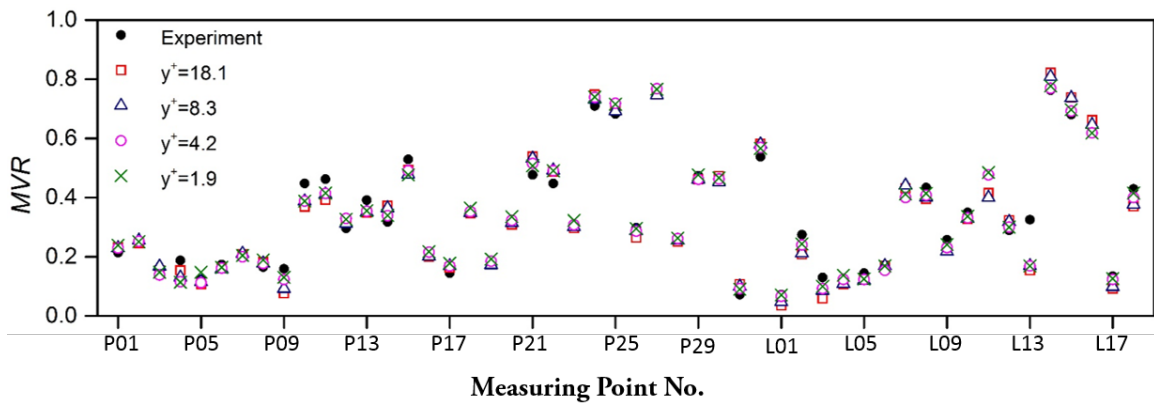


**Fig.16.** Predicted results obtained by using different near-wall mesh densities.

The predicted errors of the different near-wall mesh densities are given in Table 3. It is obvious that the values of *MAPE* and *RMSE* obtained from the cases of  $y^+=18.1$  and 8.3 are larger than that of  $y^+=4.2$  and 1.9. There are no significant differences between the cases of  $y^+=4.2$  and 1.9 because of the fact that the two-layer model has been utilized during the simulation.

**Table 3.** Predicted errors for different near-wall mesh densities

$y^+$ value	$y^+=18.1$	$y^+=8.3$	$y^+=4.2$	$y^+=1.9$
<i>MAPE</i> (%)	10.8	10.3	9.4	9.0
<i>RMSE</i> (m/s)	0.041	0.040	0.034	0.033

### 4.3 Effects of computational domain size

The size of computational domain can definitely affect the fully development of wind flow, which in turn can affect the predicted accuracy of pedestrian level wind environment. According to the BPGs, three choices have been provided for urban models of selecting proper domain cross section size: (i) the lateral boundary should be placed at least  $5H_{max}$  away from the modelled area ( $H_{max}$  is the height of tallest building in the computational model); (ii) the same cross section size as the wind tunnel test; (iii) the DBR method presented in Section 3.2, which aims to ensure the maximum blockage ratio is below 3%. In this section, the effects of above different domain cross section size on the predicted results of pedestrian level wind environment are examined based on the campus model. Apart from the aforementioned choices of domain cross section size, a larger domain cross section is also tested in this study. It should be mentioned that this section only focuses on the effects of domain cross section. The summary of the four domain sizes are presented in Table.4 and the longitudinal extension of other three cases are same as the case in Section 3.2 (see Fig.8).

**Table.4.** Summary of different computational domain sizes

Case No.	Lateral extension	Vertical extension	Maximum blockage ratio	Remark
Case 1	$5H_{max} + B_w + 5H_{max}$	$6H_{max}$	6.06%	Length based on tallest building
Case 2	5m	4m	5.3%	Same cross section as wind tunnel test
Case 3	$B_w/17\%$	$B_H/17\%$	3%	Case in Section 3.2
Case 4	$2 \times B_w/17\%$	$2 \times B_H/17\%$	0.75%	Large domain cross section

Note:  $B_w$  is the projected width of the campus model and  $B_H$  is the projected height of the campus model (see Fig.8).

The results of the four domain are shown in Fig.17. It can be observed that the results of Case 1 and Case 2 show larger discrepancies with the measurement results than that of Case 3 and Case 4 due to the small cross sections. The large deviations mainly occurred when the measuring points are on the edge of the campus model (e.g. P01-P04, L18). This suggests that the computational cross sections of Case 1 and Case 2 are not large enough for the fully development of the horizontal flow. Besides, the results obtained from Case 3 and Case 4 are almost the same, which indicates that the domain size of the Case 3 is large enough for modelling the campus model. Thus, the computational cross section

chosen by DBR method (see Section 3.2) can guarantee the fully development of the horizontal and vertical flow when the width is larger than the building height in the modelled area.

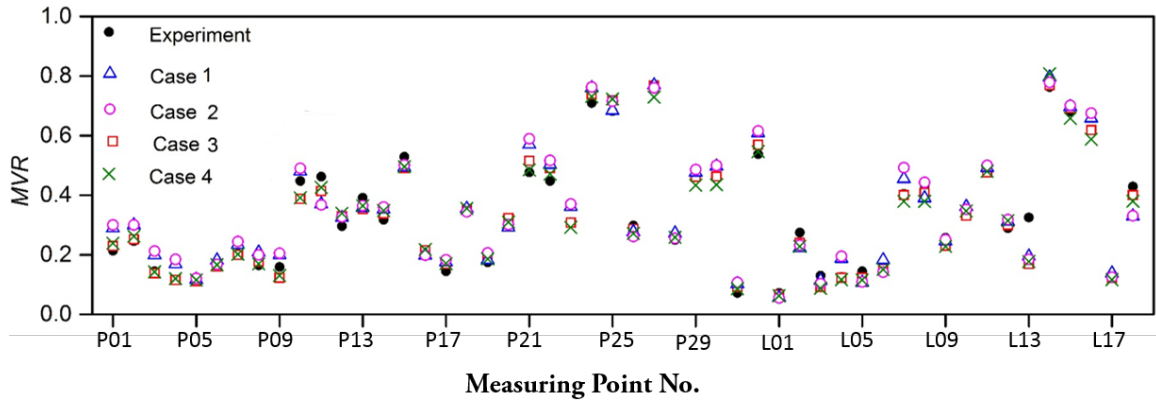


**Fig.17.** Comparison results of different domain sizes.

The predicted errors of the four cases are given in Table 5. It can be seen that the values of *MAPE* and *RMSE* obtained from Case 3 and Case 4 are almost the same. However, the results of *MAPE* and *RMSE* given by Case 1 and Case 2 are significantly larger than that of Case 3 and Case 4. The differences are mainly caused by the measuring points that located on the edge of computational model, which has been illustrated in Fig.15.

**Table 5.** Predicted errors for different domain sizes

Cases	Case 1	Case 2	Case 3	Case 4
<i>MAPE</i> (%)	12.9	11.8	9.4	9.4
<i>RMSE</i> (m/s)	0.048	0.042	0.034	0.035

## 5. Conclusions

This paper presents a study of CFD simulation of pedestrian level wind environment in a complex urban area. An effective and systematic mesh generation method is proposed and the detailed generation procedure is provided. This mesh generation method can generate a high-quality structural mesh system in a complex urban environment with full control over whole computational domain. In addition, it can ensure a sufficient near-wall mesh density without a significant increase of the total number of cells. This mesh generation method is demonstrated and evaluated based on the complex HKPolyU campus model, where wind tunnel experimental data is also available. A good agreement between CFD results and wind tunnel data is achieved, which further confirms the reliability of this method.

Based on the meshed HKPolyU campus model, the sensitivity tests of three computational parameters, namely, turbulence model, near-wall mesh density and computational domain size, are performed. Apart from the direct comparison of the CFD and wind tunnel results, MAPE and RMSE are utilized in this study to quantitatively assess the effects of the computational parameters. The main findings of the sensitivity tests can be summarized as follows:

- Among the four RANS models tested, the RNG turbulence model yields overall the best performance in predicting pedestrian level wind environment of the campus model while the SKE turbulence model cannot provide adequate predicted results.
- The near-wall mesh generation technique can provide sufficient near-wall mesh density for simulation requirement without leading to striking number of cells.
- For the computational model that has a larger model width than building height, the DBR method for choosing the domain cross section should be used to ensure the maximum blockage ratio below 3%.

In this study, only the steady-state RANS turbulence models were used. However, the proposed mesh generation method can provide a sufficient near-wall mesh density with moderate mesh number, which, therefore, also allows the application of advanced transient turbulence models, e.g., Detached Eddy Simulation (DES) model and Large Eddy Simulation (LES) model. The time needed for constructing a complex grid is also considered very important during the pre-processing stage. Thus, further studies are still needed to compare the amounts of time used by the proposed method and other meshing methods.

## **Acknowledgement**

The work described in this paper was fully supported by a grant from the Research Grants Council of the Hong Kong Special Administrative Region, China (Project No. C5002-14G).

## **Reference**

- Ai, Z.T., Mak, C.M., 2013. CFD simulation of flow and dispersion around an isolated building: Effect of inhomogeneous ABL and near-wall treatment. *Atmos. Environ.* 77, 568-578.
- Ai, Z.T., Mak, C.M., 2014. Modeling of coupled urban wind flow and indoor air flow on a high-density near-wall mesh: Sensitivity analyses and case study for single-sided ventilation. *Environ. Model. Softw.* 60, 57-68.
- Ai, Z.T., Mak, C.M., 2015. From street canyon microclimate to indoor environmental quality in naturally ventilated urban buildings: Issues and possibilities for improvement. *Build. Environ.* 94, 489-503.
- Ai, Z.T., Mak, C.M., 2017. CFD simulation of flow in a long street canyon under a perpendicular wind direction: Evaluation of three computational settings. *Build. Environ.* 114, 293-306.
- Ai, Z.T., Mak, C.M., Niu, J.L., 2013. Numerical investigation of wind-induced airflow and interunit dispersion characteristics in multistory residential buildings. *Indoor Air* 23, 417-429.

ASCE, 1999. American Society of Civil Engineers (ASCE) Manuals and Reports on Engineering Practice No. 67: Wind Tunnel Studies of Buildings and Structures. Virginia.

AWES, 2001. Assurance Manual for Wind-engineering Studies of Buildings (AWES-QAM-1).

Baker, C.J., 2007. Wind engineering—Past, present and future. *J. Wind Eng. Ind. Aerod.* 95, 843-870.

Bechmann, A., Sørensen, N.N., Berg, J., Mann, J., Réthoré, P.E., 2011. The Bolund Experiment, Part II: Blind Comparison of Microscale Flow Models. *Bound.-Layer Meteorol.* 141, 245-271.

Bennett, N.D., Croke, B.F.W., Guariso, G., Guillaume, J.H.A., Hamilton, S.H., Jakeman, A.J., Marsili-Libelli, S., Newham, L.T.H., Norton, J.P., Perrin, C., Pierce, S.A., Robson, B., Seppelt, R., Voinov, A.A., Fath, B.D., Andreassian, V., 2013. Characterising performance of environmental models. *Environ. Model. Softw.* 40, 1-20.

Blocken, B., 2015. Computational Fluid Dynamics for urban physics: Importance, scales, possibilities, limitations and ten tips and tricks towards accurate and reliable simulations. *Build. Environ.* 91, 219-245.

Blocken, B., Gualtieri, C., 2012. Ten iterative steps for model development and evaluation applied to Computational Fluid Dynamics for Environmental Fluid Mechanics. *Environ. Model. Softw.* 33, 1-22.

Blocken, B., Janssen, W.D., van Hooff, T., 2012. CFD simulation for pedestrian wind comfort and wind safety in urban areas: General decision framework and case study for the Eindhoven University campus. *Environ. Model. Softw.* 30, 15-34.

Blocken, B., Stathopoulos, T., Carmeliet, J., 2007. CFD simulation of the atmospheric boundary layer: wall function problems. *Atmos. Environ.* 41, 238-252.

Blocken, B., Stathopoulos, T., van Beeck, J.P.A.J., 2016. Pedestrian-level wind conditions around buildings: Review of wind-tunnel and CFD techniques and their accuracy for wind comfort assessment. *Build. Environ.* 100, 50-81.

Cermak, J.E., 2003. Wind-tunnel development and trends in applications to civil engineering. *J. Wind Eng. Ind. Aerod.* 91, 355-370.

Cui, D.J., Mak, C.M., Kwok, K.C.S., Ai, Z.T., 2016. CFD simulation of the effect of an upstream building on the inter-unit dispersion in a multi-story building in two wind directions. *J. Wind Eng. Ind. Aerod.* 150, 31-41.

Du, Y.X., Mak, C.M., Kwok, K.C.S., Tse, K.-T., Lee, T.-c., Ai, Z.T., Liu, J.L., Niu, J.L., 2017a. New criteria for assessing low wind environment at pedestrian level in Hong Kong. *Build. Environ.* 123, 23-36.

Du, Y.X., Mak, C.M., Liu, J.L., Xia, Q., Niu, J.L., Kwok, K.C.S., 2017b. Effects of lift-up design on pedestrian level wind comfort in different building configurations under three wind directions. *Build. Environ.* 117, 84-99.

Durbin, P.A., Medic, G., Seo, J.M., Eaton, J.K., Song, S., 2001. Rough Wall Modification of Two-Layer  $k-\epsilon$ . *J. Fluid Eng.* 123, 16.

FLUENT, 2010. ANSYS FLUENT 13.0 Theory Guide, Turbulence. ANSYS Inc. Canonsburg, PA.

Franke, J., Hellsten, A., Schlünzen, H., Carissimo, B., 2007. Best Practice Guideline for the CFD Simulation of Flows in the Urban Environment. COST Action 732: Quality Assurance and Improvement of Microscale Meteorological Models (2007). Hamburg, Germany.

Gorlé, C., van Beeck, J., Rambaud, P., Van Tendeloo, G., 2009. CFD modelling of small particle dispersion: The influence of the turbulence kinetic energy in the atmospheric boundary layer. *Atmos. Environ.* 43, 673-681.

Hang, J., Li, Y., 2010. Ventilation strategy and air change rates in idealized high-rise compact urban areas. *Build. Environ.* 45, 2754-2767.

HKSAR, Planning Department of the HKSAR.  
[http://www.pland.gov.hk/pland\\_en/info\\_serv/site\\_wind/site\\_wind/083039.html](http://www.pland.gov.hk/pland_en/info_serv/site_wind/site_wind/083039.html). Accessed in Jun. 2017.

Hong, B., Lin, B., 2015. Numerical studies of the outdoor wind environment and thermal comfort at pedestrian level in housing blocks with different building layout patterns and trees arrangement. *Renew. Energy.* 73, 18-27.

ICEM, 2010. ANSYS ICEM CFD 13.0 Tutorial Manual. ANSYS Inc. Canonsburg, PA.

Jakeman, A.J., Letcher, R.A., Norton, J.P., 2006. Ten iterative steps in development and evaluation of environmental models. *Environ. Model. Softw.* 21, 602-614.

Janssen, W.D., Blocken, B., van Hooff, T., 2013. Pedestrian wind comfort around buildings: Comparison of wind comfort criteria based on whole-flow field data for a complex case study. *Build. Environ.* 59, 547-562.

Juan, Y.H., Yang, A.S., Wen, C.Y., Lee, Y.T., Wang, P.C., 2017. Optimization procedures for enhancement of city breathability using arcade design in a realistic high-rise urban area. *Build. Environ.* 121, 247-261.

Laniak, G.F., Olchin, G., Goodall, J., Voinov, A., Hill, M., Glynn, P., Whelan, G., Geller, G., Quinn, N., Blind, M., Peckham, S., Reaney, S., Gaber, N., Kennedy, R., Hughes, A., 2013. Integrated environmental modeling: A vision and roadmap for the future. *Environ. Model. Softw.* 39, 3-23.

Lateb, M., Masson, C., Stathopoulos, T., Bédard, C., 2013. Comparison of various types of  $k-\epsilon$  models for pollutant emissions around a two-building configuration. *J. Wind Eng. Ind. Aerod.* 115, 9-21.

Launder, B.E., Spalding, D.B., 1972. *Mathematical Models of Turbulence*. Academic Press, New York.

Liu, J., Niu, J., Xia, Q., 2016. Combining measured thermal parameters and simulated wind velocity to predict outdoor thermal comfort. *Build. Environ.* 105, 185-197.

Lun, Y.F., Mochida, A., Yoshino, H., Murakami, S., 2007. Applicability of linear type revised  $k-\epsilon$  models to flow over topographic features. *J. Wind Eng. Ind. Aerod.* 95, 371-384.

Google Map, The Hong Kong Polytechnic University.  
<https://www.google.com.hk/maps/place/The+Hong+Kong+Polytechnic+University.html>. Accessed in July. 2017.

Mochida, A., Lun, I.Y.F., 2008. Prediction of wind environment and thermal comfort at pedestrian level in urban area. *J. Wind Eng. Ind. Aerod.* 96, 1498-1527.

Ng, E., 2009. Policies and technical guidelines for urban planning of high-density cities—air ventilation assessment (AVA) of Hong Kong. *Build. Environ.* 44, 1478-1488.

Niu, J.L., Liu, J.L., Lee, T.C., Lin, Z., Mak, C.M., Tse, K.T., Tang, B.S., Kwok, K.C.S., 2015. A new method to assess spatial variations of outdoor thermal comfort: Onsite monitoring results and implications for precinct planning. *Build. Environ.* 91, 263-270.

Ramponi, R., Blocken, B., 2012. CFD simulation of cross-ventilation for a generic isolated building: Impact of computational parameters. *Build. Environ.* 53, 34-48.

Richards, P., Mallinson, G., McMillan, D., Li, Y., 2002. Pedestrian level wind speeds in downtown Auckland. *Wind Struct.* 5, 151-164.

Shi, X., Zhu, Y., Duan, J., Shao, R., Wang, J., 2015. Assessment of pedestrian wind environment in urban planning design. *Landsc Urban Plan.* 140, 17-28.

Shih, T.-H., Liou, W.W., Shabbir, A., Yang, Z., Zhu, J., 1995. A new  $k-\epsilon$  eddy viscosity model for high Reynolds number turbulent flows. *Comput. Fluids* 24, 227-238.

Stathopoulos, T., 2006. Pedestrian level winds and outdoor human comfort. *J. Wind Eng. Ind. Aerod.* 94, 769-780.

Tamura, T., Nozawa, K., Kondo, K., 2008. AIJ guide for numerical prediction of wind loads on buildings. *J. Wind Eng. Ind. Aerod.* 96, 1974-1984.

Tominaga, Y., Mochida, A., Murakami, S., Sawaki, S., 2008a. Comparison of various revised  $k-\epsilon$  models and LES applied to flow around a high-rise building model with 1:1:2 shape placed within the surface boundary layer. *J. Wind Eng. Ind. Aerod.* 96, 389-411.

Tominaga, Y., Mochida, A., Yoshie, R., Kataoka, H., Nozu, T., Yoshikawa, M., Shirasawa, T., 2008b. AIJ guidelines for practical applications of CFD to pedestrian wind environment around buildings. *J. Wind Eng. Ind. Aerod.* 96, 1749-1761.

Tominaga, Y., Stathopoulos, T., 2009. Numerical simulation of dispersion around an isolated cubic building: Comparison of various types of  $k-\epsilon$  models. *Atmos. Environ.* 43, 3200-3210.

Tominaga, Y., Stathopoulos, T., 2011. CFD modeling of pollution dispersion in a street canyon: Comparison between LES and RANS. *J. Wind Eng. Ind. Aerod.* 99, 340-348.

Tsang, C., Kwok, K.C., Hitchcock, P.A., 2012. Wind tunnel study of pedestrian level wind environment around tall buildings: Effects of building dimensions, separation and podium. *Build. Environ.* 49, 167-181.

Tse, K.T., Zhang, X., Weerasuriya, A.U., Li, S.W., Kwok, K.C.S., Mak, C.M., Niu, J.L., 2017. Adopting ‘lift-up’ building design to improve the surrounding pedestrian-level wind environment. *Build. Environ.* 117, 154-165.

Tsuchiya, M., Murakami, S., Mochida, A., Kondo, K., Ishida, Y., 1997. Development of a new  $k-\epsilon$  model for flow and pressure fields around bluff body. *J. Wind Eng. Ind. Aerod.* 67, 169-182.

van Hooff, T., Blocken, B., 2010. Coupled urban wind flow and indoor natural ventilation modelling on a high-resolution grid: A case study for the Amsterdam ArenA stadium. *Environ. Model. Softw.* 25, 51-65.

Yakhot, V., Orszag, S.A., Thangam, S., Gatski, T.B., Speziale, C.G., 1992. Development of turbulence models for shear flows by a double expansion technique. *Fluid dynamics*. 4, 1510-1520.

Yang, Y., Gu, M., Chen, S., Jin, X., 2009. New inflow boundary conditions for modelling the neutral equilibrium atmospheric boundary layer in computational wind engineering. *J. Wind Eng. Ind. Aerod.* 97, 88-95.

Yoshie, R., Mochida, A., Tominaga, Y., Kataoka, H., Harimoto, K., Nozu, T., Shirasawa, T., 2007. Cooperative project for CFD prediction of pedestrian wind environment in the Architectural Institute of Japan. *J. Wind Eng. Ind. Aerod.* 95, 1551-1578.

Yuan, C., Norford, L., Britter, R., Ng, E., 2016. A modelling-mapping approach for fine-scale assessment of pedestrian-level wind in high-density cities. *Build. Environ.* 97, 152-165.